Int. J. Electrochem. Sci., 14 **(2019)** 4781 – 4798, doi: 10.20964/2019.05.67

International Journal of
ELECTROCHEMICAL
SCIENCE
www.electrochemsci.org

Excellent Lithium Metal Anode Performance via In Situ Interfacial Layer Induced by $Li_{6.75}La_3Zr_{1.75}Ta_{0.25}O_{12}$@Amorphous Li_3OCl Composite Solid Electrolyte

Yijun Tian [1, 2], *Fei Ding* [2,*], *Lin Sang* [2], *Yan-Bing He* [3], *Xingjiang Liu* [1, 2], *Qiang Xu* [1,**]

[1] School of Chemical Engineering and Technology, Tianjin University, Tianjin 300072, P. R. China.
[2] National Key Laboratory of Science and Technology on Power Sources, Tianjin Institute of Power Sources, Tianjin 300384, P. R. China.
[3] Engineering Laboratory for the Next Generation Power and Energy Storage Batteries, Graduate School at Shenzhen, Tsinghua University, Shenzhen, 518055, P. R. China.
[*]E-mail: fding@nklps.org, xuqiang@tju.edu.cn

Received: 20 April 2018 / *Accepted:* 17 May 2018 / *Published:* 10 April 2019

A LLZTO-2wt.% Li_3OCl composite solid electrolyte (LC) layer was attached to the surface of a Li metal electrode through a glass-fiber-paper (GF)-supported method to form a stable in situ reaction interfacial layer between the Li metal anode and an organic liquid electrolyte in Li metal batteries. The Li metal anode modified by GF-LC showed excellent cycling stability in a Li metal symmetric battery (over 1100 h stable cycles at 1 mA cm^{-2} / 1 mA h cm^{-2} with less corrosion of Li metal anode) and Li-Cu battery (over 300 h cycles at 1 mA cm^{-2} / 1 mA h cm^{-2} with Coulombic efficiency of 99.0%). The superior stability and dendrite-free mechanism of the GF-LC-modified Li metal anode is related to the reduced direct contact area and less corrosive side reactions between the organic electrolyte and the Li metal anode. Based on the excellent stability of the GF-LC-modified Li metal anode, a Li-S battery was assembled to research the effect of the GF-LC modified Li metal anode on cycling stability. Compared with Li-S batteries modified by pristine and GF-modified Li metal anodes, the GF-LC-modified Li-S battery showed better cycling stability and longer cycling life.

Keywords: Lithium Metal Anode; $Li_{6.75}La_3Zr_{1.75}Ta_{0.25}O_{12}$@Amorphous Li_3OCl Composite Solid Electrolyte; Interfacial Layer; Li-S battery

1. INTRODUCTION

Traditional Li ion batteries associated with intercalation chemistry are meeting more challenges in the increasing energy density demand with the rapid development of advanced portable devices,

electric vehicles (EV), hybrid EVs, and large-scale grid energy storage[1, 2]. Thus, Li–S and Li–O_2 batteries based on Li metal anodes with high theoretical capacity have attracted enormous attention[3, 4]. Li metal anodes are the best and ultimate form of high-capacity anode material for Li ion batteries. The Li metal anode has ultrahigh theoretical capacity (3860 mA h g^{-1}) and low standard electrode potential (3.040 V vs. SHE)[5]. The commercialization of batteries based on Li metal anodes remains unsuccessful, however, mainly because of the uneven deposition/dissolution of Li metals, low efficiency and short cycle life that derives from uncontrolled Li dendrite growth and the successive side reactions between Li metals and electrolytes[6, 7]. Li metal anodes with high reactive action are more likely to react easily with most organic electrolyte solvents, Li salts, solid ceramics and polymer electrolytes to form an unstable and thick solid electrolyte interlayer (SEI). However, the SEI layer usually is effortlessly broken in the Li deposition process, and the current density in the surface of the Li metal is not distributed homogeneously so that Li dendrites are generated easily and grown quickly[8]. Then, a new SEI layer is more likely to generate again on the Li dendrites. Continuous damage of the SEI layer and germination of Li dendrites in the cycling process of batteries can cause uneven deposition/dissolution of Li metals and provide more activated area for the side reactions between Li metals and electrolytes[9], which could consume the Li ions continuously and cause lower Coulombic efficiency and short circuits in the long-term cycling due to uncontrolled Li dendrite growth[10, 11].

Numerous researchers have focused on addressing these issues to implement the commercialization of Li metal anodes, mainly in two aspects: the control of Li deposition morphology to constrain Li dendrite growth[12]; and the improvement of a stable SEI layer to prevent Li metal anodes from continuous breakage and repair of the SEI layer[13]. The various strategies related with these issues have been mentioned, which primarily include the modifications of separators with various nanoparticles[14], such as Al_2O_3[15], SiO_2[16], h-BN[17] and MOFs[18], the Li metal anode with 3D structure and nanostructure[19, 20], the electrolyte with additives[21] and the use of artificial interface layers such as Li_3PO_4[22] and LiF[23]. These methods were used to protect Li metal anodes, control the growth of Li dendrites and improve the stability of the SEI layer during electrochemical discharging/charging cycles. Li metals with unstable character in thermodynamics could, however, easily react with organic solvents that could make it difficult to passivate the surface of the Li metal anodes and obtain a stable SEI layer, especially for large current density.

Solid electrolytes have attracted increased research due to their safety and wider electrochemical windows [24, 25]. More importantly, Li metals can be used directly as anodes for all-solid-state batteries. Solid electrolytes suffer, however, from low ionic conductivities, high interfacial resistance and continuous reactions with Li metal anodes so that it is difficult to implement the commercialization of all-solid-state batteries[26, 27]. However, solid electrolytes, including ceramic and polymer electrolytes with high mechanical strength, have been used as a protective interfacial layer for Li metal anodes in liquid electrolytes to control the growth of Li dendrites due to the decreased contact area between the Li metal and the liquid electrolyte[28, 29]. Whereas most solid electrolytes are unstable with Li metals, such as sulfide-based electrolytes[30] and most oxides (LATP, LLTO, etc.)[31], LLZO, as one of the few solid electrolytes that are stable with Li metals, has been selected to modify the Li metal anode[32]. The garnet LLZO cannot, however, be wetted by the Li

metal until heating for a long period (24-168 h) at 300-350 °C, much higher than the Li metal melting point of 180.5 °C, which causes much higher interfacial resistance between the Li metal and the LLZO electrolyte layer[33, 34]. That is not ideal for batteries using Li metals as anodes.

Recently, we studied a garnet and Antiperovskite composite solid electrolyte LLZTO-2wt.% Li_3OCl with higher Li ion conductivity (2.26×10^{-4} S cm^{-1}), which could be easily wetted by Li metals and has excellent interfacial stability with Li metal anodes in all-solid-state Li symmetric batteries owing to the formation of interfacial layers [35]. This layer could decrease the interfacial resistance, suppress the growth of Li dendrites and assure that there is an even Li ion transport through the interface between the Li metal anode and the LLZTO-Li_3OCl solid electrolyte.

In this paper, we introduce this interfacial layer formed through in situ reactions between Li metals and LLZTO-Li_3OCl solid electrolyte layers into batteries with liquid electrolytes. The interfacial layer induced by Garnet and Antiperovskite Composite Solid Electrolyte was demonstrated to be stable in the liquid electrolyte for over 1000 h of even deposition/dissolution of the Li metal for a Li metal symmetric battery (1 mA cm^{-2} / 1 mA h cm^{-2}) and over 150 cycles of Li deposition and removal on Cu foil with a Coulombic efficiency 99.0% (1 mA cm^{-2} / 1 mA h cm^{-2}). There was no obvious corrosion, dendrites and side-reaction products in the bulk Li metal anode modified with glass fiber paper / LLZTO-2wt.% Li_3OCl composite solid electrolyte (GF-LC) for a Li symmetric battery after over 1000 h cycles compared with pristine and glass fiber paper (GF)-modified Li metal anodes. Moreover, the modified Li anode with GF-LC enabled dense Li deposition and no obvious rising electrochemical resistance was observed in the over 1000 h cycles for the Li symmetric battery. Based on the newly modified method for the Li metal anode, a Li-S battery was successfully assembled and operated using a modified Li metal anode with GF-LC, liquid electrolyte and a sulfur cathode.

The comparison schematic of the GF layer and GF-LC layer coated on Li metals in the cycling process and corresponding side-view SEM images of Li metal anodes of Li symmetric cells after ~1000 h cycling at a current density of 1 mA cm^{-2} are shown in Fig. 1. The Li metal electrode coated with GF paper facilitated redistribution of the Li ions concentrated by the protuberances of Cu foil electrodes or Li foil electrodes, which may lead to dendrite-free Li deposition and high Coulombic efficiency to some extent[36]. Owing to the superior wettability with organic liquid electrolytes[36], however, GF could not hold back the direct contact between the Li metal and liquid electrolyte, which may cause side reactions on the surface of the Li metal in the charge/discharge cycling process. So, the bulk Li metal coated by GF could experience serious corrosion (Fig. 1b) after long-term (1000 h) cycling at 1 mA cm^{-2}. By contrast, the Li metal of the Li-LC-GF|GF-LC-Li symmetric cell had hardly any corrosion after over 1000 h cycling (Fig. 1d), which is attributed to the existence of the LLZTO-Li_3OCl layer. As seen in the schematic and side-view SEM images shown in Fig. 1c, d, the surface of the Li metal electrode was coated fully with the LLZTO-Li_3OCl layer owing to the superior lithiophilicity. Furthermore, the interaction between composite solid electrolyte and Li metal could form a stable interfacial film in the interface, as shown in our previous work. Thus, the existence of LLZTO-Li_3OCl may reduce direct contact of liquid electrolytes and Li metal electrodes to decrease corrosive side reactions between them. In addition, the preferable Li ionic conductivity and electronic resistivity for the LLZTO-Li_3OCl protective layer permits Li ionic transportation and inhibits electronic transportation. Therefore, the Li metal is deposited beneath the LLZTO-Li_3OCl protective

layer (including the in situ interfacial layer) rather than on the top of the LLZTO-Li_3OCl layer, which distinctly decreased the possibility of dendrite germination and corrosion side-reactions[37].

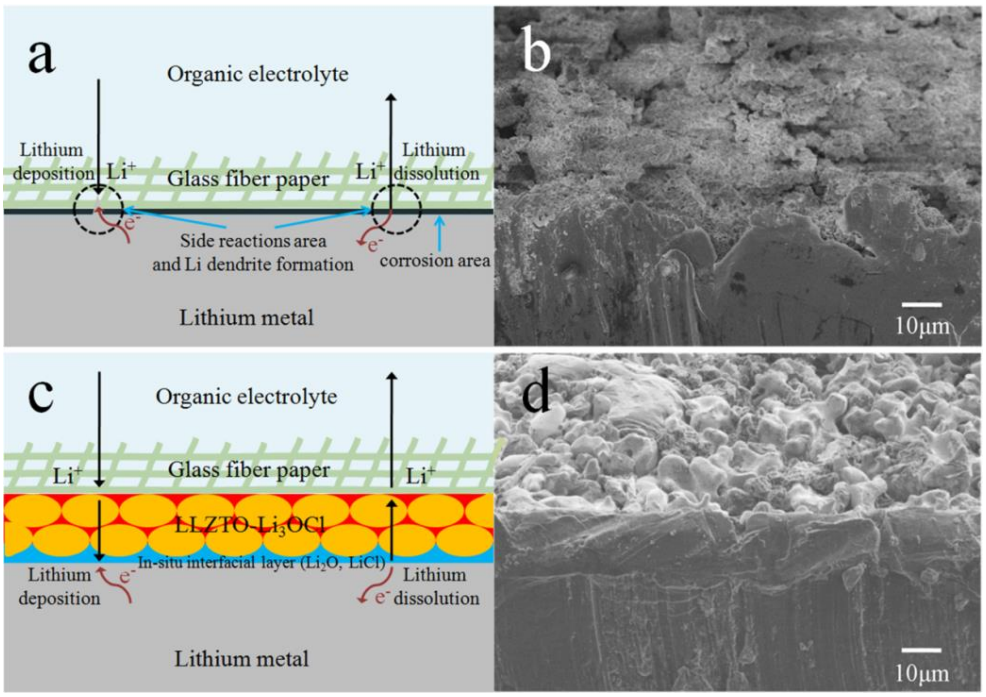

Figure 1. Schematics of Li-ion transfer in the interface between (a) GF and Li metal anode, (c) GF-LC and Li metal anode. (b) Side-view SEM images of the GF modified Li metal electrode for Li symmetric battery after 1000 h cycles correlating to (a) schematic. (d) Side-view SEM images of the GF-LC modified Li metal electrode for Li symmetric battery after 1100 h cycles correlating to (c) schematic.

2. EXPERIMENT

2.1 Preparation of the LLZTO and Li_3OCl solid electrolytes

LLZTO and Li_3OCl powder samples were prepared using a simple solid-state synthetic technique described in our previous research [35].

2.2 Preparation of the GF-LC

The as-prepared LLZTO and Li_3OCl powders were crushed by pestle and mixed adequately in a weight ratio of 40:1 in an agate mortar. They were then ultrasonically dispersed in THF for 3 hours (1.5 mg of the mixture per 1 mL of solvent) to form a slurry. Then, several droplets of the LLZTO/Li_3OCl slurry were placed onto the surface of GF paper with a pipette, and the THF was left to evaporate at room temperature for a few minutes. This procedure was repeated several times until the LLZTO/Li_3OCl composite solid electrolyte covered the surface of GF paper fully. Next, the GF paper coated with LLZTO/Li_3OCl was dried at 100 °C for 1 h under vacuum then sintered at 350 °C for 12 h in an argon-filled glove box with less than 0.1 ppm oxygen and 0.1 ppm H_2O. Finally, the white GF-

LC was obtained, and the GF-LC modified Li metal electrode was formed by attaching Li foil to the LC side of GF-LC.

2.3 Preparation of the sulfur cathode and coin-type battery

The S/C composite was prepared by a conventionally-used melting diffusion strategy with a mixture of sulfur and Super P in the weight ratio of 7:3 followed by co-heating at 155 °C for 12 h. The cathode slurry was prepared by mixing 90 wt% S/C composite, 10 wt% polyvinylidene difluoride (PVDF) as binders dissolved in N-methyl-2-pyrrolidone (NMP) as solvent and stirring for over 10 h. The cathode films were produced by coating the slurry onto aluminum foil. After the solvent was evaporated at 50 °C, the electrode was cut into discs 20 mm in diameter and dried at 70 °C for 12 h under vacuum. The areal sulfur loading in the cathode was approximately 2 mg cm^{-2}. The electrolyte was 1 M $LiN(CF_3SO_2)_2$ (LiTFSI) and 2wt% lithium nitrate ($LiNO_3$) dissolved in a mixed solvent of 1,3-dioxolane (DOL) and dimethyl ether (DME). The CR2040 type coin batteries were assembled in a glove box with oxygen and water contents less than 0.1 ppm using a commercial polypropylene (PP) membrane as the separator and pristine lithium foils, GF or GF-LC modified Li foils as the counter electrode.

Symmetric Li metal batteries were assembled by using two pristine lithium foils, GF modified Li foils or GF-LC modified Li foils, a separator, and organic liquid electrolyte to prepare three types of Li metal symmetric batteries. The three types of Li | Cu cells were also assembled by using the bare Cu foil, GF modified foil or GF-LC modified Cu foil, a separator, and liquid electrolyte. The performance of all cells was tested using a LAND electrochemical testing system.

2.4 Structural and electrochemical characterization

The cross-section scanning electron microscopy (SEM) images were measured on a field-emission scanning electron microscope (HITACHI S-4800). Powder X-ray diffraction (TTR III, Cu Kα) was employed to monitor the phase formation. The distribution of the Li metal elements was measured by energy dispersive spectroscopy (EMAX 7593-H). X-ray photoelectron spectroscopy (XPS) was performed with a PHI 5000 Versa Probe II. Cyclic voltammetry (CV) was carried out on a Princeton electrochemical workstation at a scan rate of 0.1 mV s^{-1} from 1.7 V to 2.8 V for Li-S batteries. The galvanostatic charge and discharge tests of Li-S batteries were conducted by using a CT2001 multichannel battery tester at room temperature in a voltage range of 1.7-2.8 V (vs. Li/Li^+) at 0.2 C (1 C=1670 mA g^{-1}).

3. RESULTS AND DISCUSSION

3.1 Structural characterization of the GF-LC

The characteristics of the LLZTO-Li_3OCl composite solid electrolyte were studied in detail in our previous research (*refer 35*). The GF paper heated at 350 °C without any changes was selected as

reaction supporter of LC composite solid electrolyte, and the LC was coated onto a commercial GF paper to prepare the GF-LC as interlayer between Li metal and liquid electrolyte. The surface morphologies of the pristine and LC-coated GF papers are shown in the SEM images (Fig. 2a, 2b). The insets in Fig. 2a, 2b are digital photos of GF and GF coated with LLZTO-Li_3OCl composite solid electrolyte, respectively. Compared with fiber-weaved pristine GF paper, the LC-coated GF was clearly distinguished and fully coated by LLZTO-Li_3OCl particles. As is shown in the cross-section SEM of the LC-coated GF paper, the LLZTO-Li_3OCl layer was approximately 20 μm thick, and the LLZTO-Li_3OCl particles attached closely to the surface of the glass fiber paper. The XRD patterns of LLZTO powder, Li_3OCl powder, GF paper surface, and GF-LC surface are shown in Fig. 2d. The LLZTO and Li_3OCl solid electrolytes were standard garnet and antiperovskite structure, respectively [32, 39]. The GF papers before and after heating at 350 °C both displayed an amorphous feature, and there were no other XRD peaks after heating, which indicates the GF was stable at 350 °C and why we selected it as the reaction supporter. The GF-LC showed a garnet structure similar to LLZTO but with lowered crystallinity, which is attributed to the formation of amorphous Li_3OCl in the preparation process of the LC composite solid electrolyte mentioned in *refer 35*. Thus, the surface of the GF paper was coated fully by a thin LLZTO-Li_3OCl composite solid electrolyte layer.

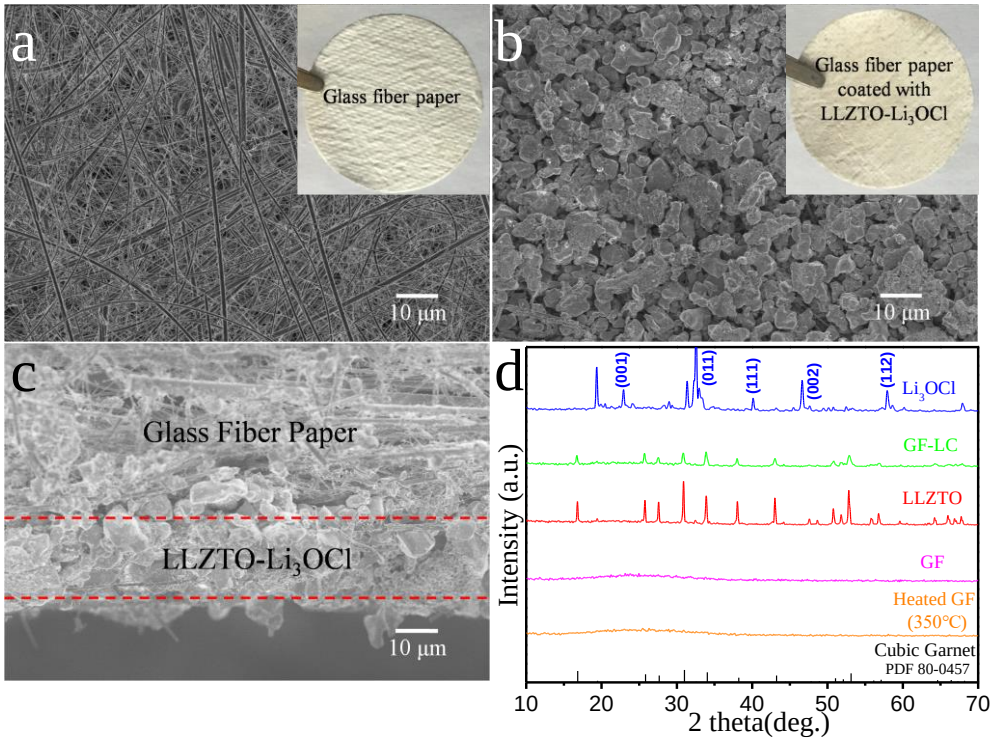

Figure 2. a, b, Top-view of SEM images of GF (a) and GF-LC (b). Insets are digital photos of glass fiber paper and glass fiber paper coated with LLZTO-Li_3OCl composite solid electrolyte, respectively. **c**, Cross-sectional view of GF-LC. **d**, XRD patterns of LLZTO powder, Li_3OCl powder, GF paper before and after heating at 350 °C, and GF-LC surface.

3.2 Electrochemical characterization and stable mechanism *of GF-LC modified Li metal anode*

The interfacial layer formed in the solid battery with LLZTO-Li_3OCl solid electrolyte showed a positive effect on the Li metal anode [35]. To determine if the effect was maintained in the liquid electrolyte, we assembled symmetric Li metal batteries with the structure of Li metal-LC-GF/separator/GF-LC-Li metal and 1 M lithium bis(trifluoromethane) sulfonimide (LiTFSI) in 1,3-dioxolane (DOL)/1,2-dimethoxyethane (DME) (1:1 volumetric ratio) solution with 2wt% $LiNO_3$ additive used as the electrolyte. We carried out direct-current (dc) Li plating and stripping experiments to investigate the cycling stability of Li metal anodes. The EIS of three types of symmetric batteries with GF-LC modified, GF-modified and pristine Li metal electrodes are shown in Figure S1. The GF-LC-modified cell exhibited the largest bulk resistance (2.64 Ω) from the high-frequency x–intercepts but the lowest interface impedances (6.74 Ω) from the distinct arc, while the GF-modified cell showed the largest interface impedance (9.42 Ω), which indicates the existence of GF and LC could increase bulk resistance and GF can increase the interfacial impedance of Li symmetric cells, while the existence of LC could effectively decrease interfacial resistance. Thus, the GF-LC could not restrict the diffusion of Li^+ due to the existence of a solid electrolyte layer compared with GF. Three types of symmetric batteries were cycled at 1 mA cm^{-2} / 1 mA h cm^{-2} for long-term cycling (Fig. 3a). The polarization voltage for three types of batteries was in accordance with total resistance in Figure S1. The cells with GF-modified and pristine Li metal electrodes could be cycled for 300 h (1 h per half a cycle) with stable voltage responses of 20 mV and 50 mV, respectively, before the voltage responses became noisy and large. In contrast, the cell with a GF-LC-modified electrode displayed an extremely stable cycling with small voltage polarization of approximately 50 mV for more than 1100 h, corresponding to more than 500 consecutive cycles. As the insets of Fig. 3a show, for every cycle of Li plating and stripping process, the voltage response of the cell with GF-LC was superiorly stable, even after over 1000 h cycles, compared with the other two types of cells, which indicates that the lower interfacial impedance and a stable interface between the Li metal and electrolyte during cycling were obtained. The cyclability performances for the three types of Li metal symmetric cells at different current densities (Fig. 3b.) and 2 mA cm^{-2} / 2 mA h cm^{-2} (Figure S2) showed that the GF-LC-modified Li metal displayed excellent cyclability and extremely stable voltage polarization at different current densities from 0.5 mA cm^{-2} to 5 mA cm^{-2} compared with the other two types of Li metals. The lower interfacial impedance and extremely stable interface for the GF-LC-modified Li metal electrode is possibly related with the formation of an interfacial layer induced by LLZTO-2wt% Li_3OCl with high lithiophilicity, which could avoid direct contact between the liquid electrolyte and Li metal so as to reduce corrosive side reactions (digital photos of Li metals after cycling for three types of symmetric cells are shown in Figure S3) and prolong the cycling life of the Li metal cell.

Li | Cu cells were also conducted at a current density of 1 mA cm^{-2} and capacity of 1 mA h cm^{-2} to compare the Coulombic efficiencies and to evaluate the reaction reversibility and their stability upon cycling of Li plating/stripping on bare Cu foil, GF-modified Cu foil and GF-LC-modified Cu foil. As shown in Fig. 3c, the Li | bare Cu cell showed inferior Coulombic efficiency and electrochemical cycling stability with a short life (~95% for about 5 cycles and under 90% after 17 cycles), while the Li | GF-modified Cu cell improved Coulombic efficiency and electrochemical

cycling stability with longer life (~97% for about 70 cycles and under 90% after 78 cycles), which is in accordance with *refer 36*. The Li | GF-LC-modified Cu cell displayed, however, a more stable electrochemical cycling, higher Coulombic efficiency and longer cycling life (~99% for about 150 cycles and under 90% after 165 cycles) compared with the Li | GF-modified Cu cell.

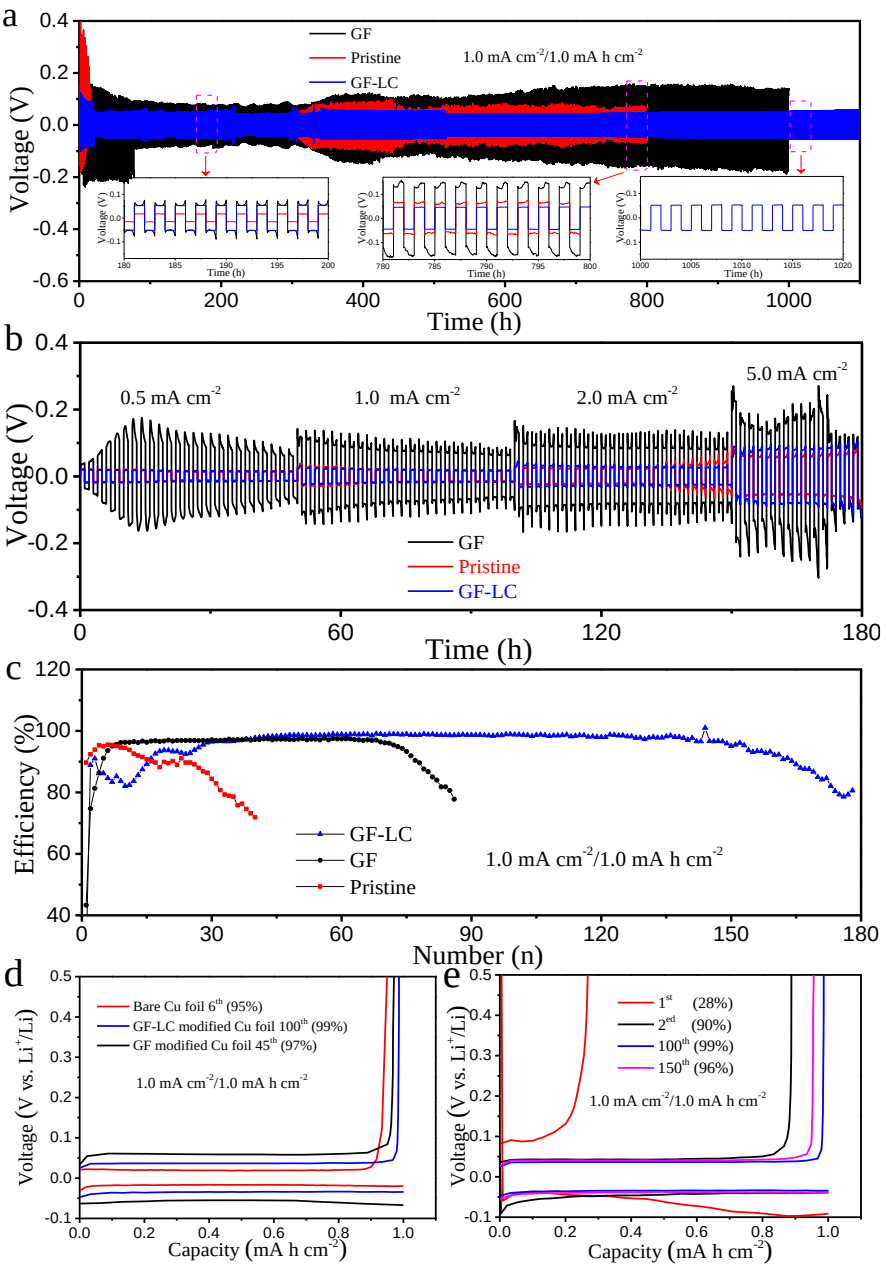

Figure 3. a, Galvanostatic cycling performance of Li metal symmetric cells with pristine (800 h), GF- (1000 h) and GF-LC- (1100h) modified Li metal anodes at a current density of 1 mA·cm^{-2} for 1 mA·h·cm^{-2}. The insets are enlarged voltage profiles for specific cycles. **b,** Cyclability of the three types of symmetric cells for 180 h with different current densities. **c,** Comparison of the Coulombic efficiency of Li deposition on bare Cu foil, GF-modified Cu foil and GF-LC-modified Cu foil electrode at a current density of 1 mA·cm^{-2} and capacity of 1 mA·h·cm^{-2}. **d**, The polarization of the plating/stripping for bare, GF-modified, and GF-LC-modified Cu foil electrode in stable cycling stage. **e,** The polarization of the Li plating/stripping for GF-LC-modified Cu foil electrode in different cycles.

The comparison of charge-discharge profiles for the three types of Li-Cu cells in the stable stage is shown in Fig. 3d. The voltage hystereses (defined as the difference between the Li depositing and Li stripping potential plateaus) of Li | bare Cu cell, Li | GF-LC-modified Cu cell and Li | GF-modified Cu cell were 40 mV, 71 mV and 122 mV, respectively. Moreover, the Li | GF-LC-modified Cu cell displayed the most even charge-discharge potential plateaus compared with the Li | bare Cu cell and the Li | GF-modified Cu cell. Fig. 3e shows the voltage hysteresis of the Li plating/stripping for GF-LC-modified Cu foil electrode in different cycles. The first cycle, with a Coulombic efficiency of just 28%, is attributed to the formation of an SEI layer. The stable voltage hysteresis of approximately 70 mV was maintained after the second cycle for 160 cycles. The lower Coulombic efficiency, voltage hysteresis and poor cycling stability for pristine Li metal electrodes indicate that the SEI layer is generated and broken repeatedly, which leads to continual consumption of electrolyte and corrosion of bulk Li metal owing to the side reaction[38]. For Li metal electrodes modified by GF, the Coulombic efficiency and cycling stability were improved due to the homogeneous distribution of Li ions mentioned in *refer 36*[36]. However, the side reactions could not be vanquished because of the direct contact of unstable Li metal thermodynamic and organic solvents. Thus, it was difficult to obtain a sufficiently passivated Li metal surface in liquid solutions. The LLZTO-Li_3OCl layer with super lithiophilicity has, however, a superior Li ionic conductivity and inferior electronic conductivity so that it allows Li ion transport while inhibiting the electron transport. Therefore, the Li metal is deposited between the LLZTO-Li_3OCl layer and the Li metal substrate, which reduces the direct contact area between the Li metal and the organic solvents so as to decrease the possibility of side reactions. Furthermore, the interaction between LLZTO-Li_3OCl and Li metals could form a stable interfacial layer to suppress the growth of Li dendrites, which was proven in *Refer 35*. The factors above suggest that Li metal electrodes modified by GF-LC may significantly decrease the possibility of corrosive side reactions and dendrite formation, which could lessen the consumption of electrolyte and corrosion of Li metal so as to prolong the cycling life of Li metal batteries.

To further investigate the stable mechanism of over 1100 h cycles for the symmetric battery with GF-LC-modified Li metal electrodes, the three types of symmetric cells after cycling in Fig. 3a, 3b were disassembled carefully to obtain Li metal electrodes, separators and GFs. The Li metal with metal luster and less atrament (products of side reactions), the separator and GF with no damage and less atrament for the symmetric cell with GF-LC modified Li metal electrodes are shown in digital photos compared with those of the symmetric cells with GF-modified and pristine Li metal electrodes (insets of Fig. 3a, 3b and 3c), which indicates that the Li dendrite impaled the separator and that many side reactions occurred between Li metals and organic electrolytes for GF-modified and pristine Li metal electrodes without modification of the LLZTO-Li_3OCl layer. More interestingly, as shown in these photos of the three types of Li metals after cycling, the side-reaction corrosion for pristine Li metal was heterogeneous, but it was homogeneous for the GF-modified Li metal, which also demonstrates the uniformly distributed Li^+ caused by GF mentioned in *refer 36*[36].

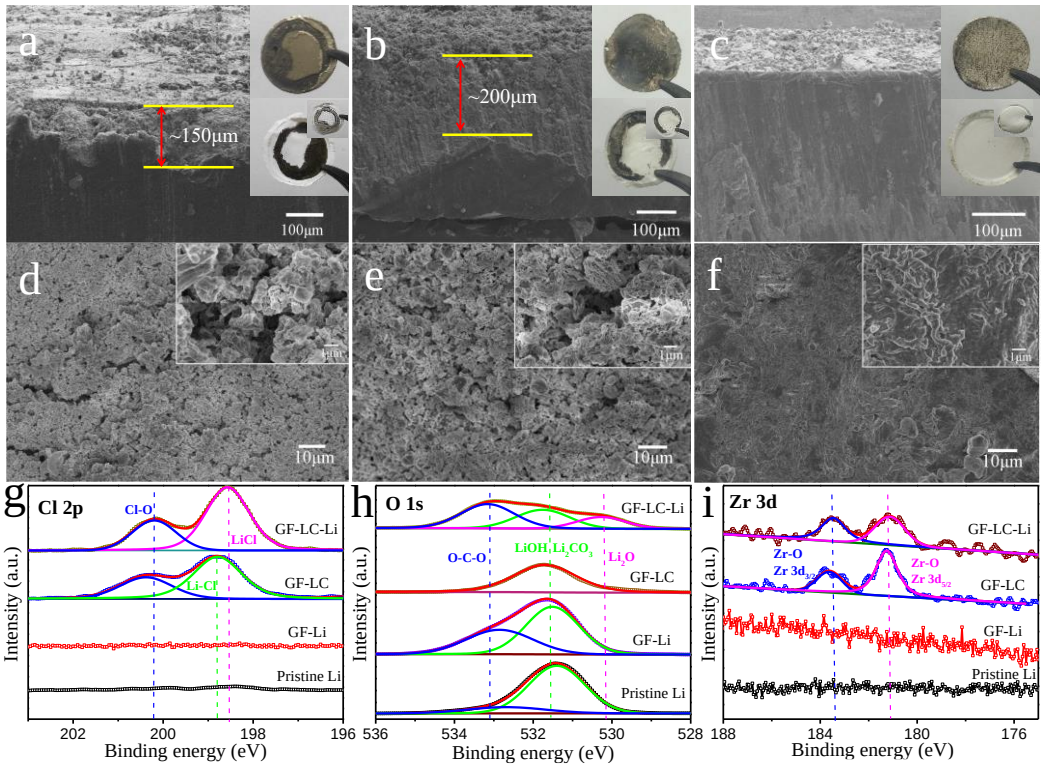

Figure 4 a, **b**, **c** Side-view SEM images and **d**, **e**, **f** top-view SEM images of the pristine (a, d), GF modified (b, e) and GF-LC modified (c, f) Li metal plates after 800 h, 1000 h and 1100 h cycles for Li symmetric batteries, respectively. Insets in **a**, **b** and **c** are digital photos of Li metal plates and separators for Li symmetric batteries with pristine, GF- and GF-LC-modified Li metal electrodes disassembled after 800 h, 1000 h and 1100 h cycles, respectively, and the insets in **d**, **e**, **f** are enlarged SEM images. **g**, Cl 2p, **h**, O 1s and **i**, Zr 3d XPS spectra of the GF-LC surface and the pristine, GF modified and GF-LC modified Li metal surface for symmetric Li metal cells after 800 h, 1000 h and 1100 h cycling, respectively, at a current density of 1 mA cm^{-2}.

SEM imaging was conducted to examine the morphology and microstructure of Li metals for three types of Li symmetric batteries after 800 h (pristine cell), 1000 h (GF) and 1200 h (GF-LC) cycling (Fig. 4a-4f). The Li metals of pristine (Fig. 4a and 4d) and GF-modified (Fig. 4b and 4e) symmetric cells displayed a spongy and porous structure with a thickness of ~150 μm and ~200 μm, respectively, which indicated that the bulk Li metals suffered from serious corrosion and consumption during long-term cycling owing to the successive side reactions between the liquid electrolytes and Li metals. In contrast, the Li metal electrodes modified by GF-LC (Fig. 4c and 4f) still displayed a smooth and dense surface without obvious corrosion and dendrite structure after 1100 hours of cycling, which demonstrates that the dense in situ reaction interface of Li metals modified by GF-LC could protect Li metals from corrosion due to the continual side reactions. In addition, because of the super lithiophilicity of the LLZTO-Li_3OCl layer, many LLZTO-Li_3OCl particles were retained on the surface of the Li metal, even if the Li metal was washed repeatedly with DOL solution, which further manifests the formation of an interfacial layer induced by an in situ reaction of LLZTO-Li_3OCl composite solid electrolyte with Li metal. The XPS spectra of the Li metal electrode surface for the three types of symmetric cells mentioned above and the GF-LC surface shown in Fig. 4g-4i and Figure

S4 indicate the existence of LC (peaks in Zr 3d spectrum at 183.5 eV and 181.2 eV corresponding to Zr-O, peak in Cl 2p spectrum at 200.2 eV corresponding to Cl-O) and Li_2O, a LiCl interfacial layer (peaks in Cl 2p and Li 1s spectra at 198.5 eV and 55.9 eV, respectively, corresponding to LiCl, peak in O 1s spectrum at 530.1 eV corresponding to Li_2O) on the surface of the GF-LC modified Li metal electrode. From Figure S5, the dense and smooth surface morphology and correlating EDX mapping of Li metal after 1000 h of successive Li plating/stripping process further manifest the protective mechanism of the LC composite solid electrolyte layer with super lithiophilicity mentioned in *refer 35*. Thus, the in situ reaction interfacial layer induced by the innovative GF-LC strategy could restrain Li dendrite growth and reduce corrosive side-reactions between the organic electrolyte and the Li metal electrode. There are many modified strategies of artificial interface layers and Li plating matrices to improve Li metal anode performance. For example, Li_3PO_4[22], LiF[23] and Cu_3N+ styrene butadiene rubber[40] as artificial interface layers improve the cycling stability of Li metal anodes, GF[36], N-doped graphene[41] and functional metal–organic frameworks[42] as the Li plating matrices to regulate Li metal nucleation and suppress dendrite growth. Compared with the above modified strategies of Li metal anodes, the GF-LC method combines both advantages through the in situ reaction interfacial layer and the GF matrix. Thus, the Li metal anode modified by GF-LC exhibits excellent cycling stability and life. Moreover, Table 1 lists comparisons of different strategies for improving the performance of Li metal electrodes. Compared with other strategies, the GF-LC method exhibits extreme advantages for both Li symmetric and Li | Cu cells.

3.3 The assembly of Li-S battery with GF-LC modified Li metal anodes

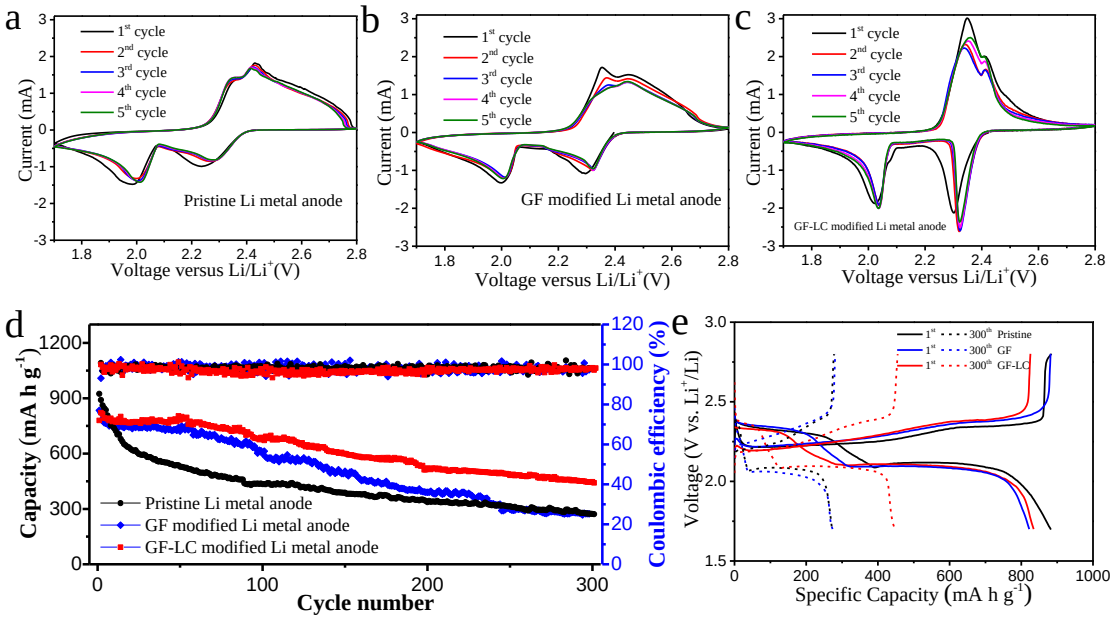

Figure 5 a, b, c, CV profiles of Li-S batteries with pristine (a), GF modified (b) and GF-LC modified (c) Li metal anode. **d, e,** Cycling performance (d) and Charge/discharge curves at initial and terminal cycles (e) of the Li-S batteries with pristine, GF-modified and GF-LC-modified Li metal anodes at a charge/discharge current density of 0.2 C.

The cyclic voltammogram (CV) profiles of Li-S batteries with pristine, GF-modified and GF-LC-modified Li metal anodes are shown in Fig. 5a, 5b, and 5c, respectively, to identify the redox reactions. As shown, all the batteries had two pairs of redox peaks correlating to the reaction between S_8 molecules and Li_2S_4, as well as the transformation between soluble Li_2S_4 and insoluble Li_2S_2 or Li_2S, respectively, which indicates that GF and GF-LC on the surface of Li metal anodes do not change the electrochemical reactions in the electrochemical window (1.7 V-2.8 V) for Li-S batteries. In addition, compared with the CV profiles of batteries with pristine and GF-modified Li metal anodes, the battery with the GF-LC-modified Li metal anode displayed two pairs of more prominent redox peaks with higher redox currents, which may be attributed to the fewer side reactions and faster Li^+ diffusion between the Li metal anode and organic electrolyte with the existence of LLZTO-Li_3OCl composite electrolyte on the surface of the Li metal anode. These results are in accord with those in symmetric Li metal batteries.

Li-S batteries with pristine, GF-modified and GF-L- modified Li metal anodes and S/Super P (70% S Figure S6a) cathodes were assembled to further manifest the application of the newly developed interface protective mechanism for Li metal electrodes in the practical use of batteries. The cycling performance and charge/discharge profile of Li–S batteries with different Li metal electrodes at 0.2 C are shown in Fig. 5d and 5e. As seen in Fig. 5d and 5e, compared with the Li-S batteries with GF- and GF-LC-modified Li metal anodes, the specific capacity of the battery with the pristine Li metal anode decreased sharply, especially before 100 cycles from 924.1 mA h g^{-1} to 434.5 mA h g^{-1} at 0.2 C (1 C=1670 mA g^{-1}) with a capacity retention of only 47.0%, while from 834.4 mA h g^{-1}, 822.2 mA h g^{-1} to 602.5 mA h g^{-1}, 703.5 mA h g^{-1} a capacity retention of 72.2% and 85.6% for the GF-modified and the GF-LC-modified Li-S batteries, respectively, was observed. The capacity decreased, however, more rapidly to 273.5 mA h g^{-1} after 100 cycles for the GF-modified Li-S battery, with a capacity retention of only 32.8% after 300 cycles, which is comparable with that of the Li-S battery with a pristine Li metal anode (274.0 mA h g^{-1} with capacity retention of 29.7%) and worse than that of the GF-LC-modified Li-S battery (450.9 mA h g^{-1} with capacity retention of 54.9%). The GF-modified Li metal anode could suppress the ‘shuttle effect’ to a certain extent (before 100 cycles) owing to the even distribution of Li ions on the surface of Li metal anode mentioned in *refer 36*, but it could not escape the corrosion of the Li metal anode because of the direct contact and side reactions between organic electrolytes, including dissolved lithium polysulfides and Li metal anodes. Thus, the rapid capacity fading after 100 cycles was discovered. As mentioned above, the interfacial layer induced by garnet and antiperovskite composite solid electrolytes could, however, decrease the direct contact area and reduce corrosive side reactions between organic electrolytes and Li metal anodes so as to reduce the corrosion of Li metal anodes and the consumption of electrolyte. Similarly, the contact areas of Li metal anodes and lithium polysulfides is restricted, which may suppress corrosive reactions between Li metal anodes and lithium polysulfides to maintain a smooth surface of the Li metal anodes and promote more reutilization of lithium polysulfides to reduce the capacity loss of S in the subsequent cycles. Thus, the ‘shuttle effect’ and rapid capacity fading could be suppressed significantly to prolong cycling life.

4. CONCLUSION

In summary, the interfacial layer induced by LLZTO-Li_3OCl composite solid electrolytes with Li metals was successfully applied to modify a Li metal anode through a simple and novel GF-LC method. The GF-LC-modified Li metal anode displayed higher stability in organic liquid electrolyte for a symmetric Li metal battery, Li-Cu battery and Li-S battery compared with the primitive Li anode and GF-modified Li anode. First, the existence of an LLZTO-Li_3OCl layer with high Li^+ conductivity and electronic resistivity could not restrict the diffusion kinetics of Li^+ but inhibited the electron transmission so that the Li metal was deposited underneath the composite solid electrolyte, which may suppress the growth of Li dendrites owing to a non-uniform deposition of Li. Second, the composite solid electrolyte could decrease the direct contact area of organic electrolytes and Li metal anodes so as to reduce the corrosive side reactions between organic electrolytes, including lithium polysulfides and Li metal anodes in Li-S batteries, which could reduce the corrosion of Li metal anodes and the consumption of electrolytes to improve cycling stability and the life of batteries. Third, the GF and LC are fireproof materials, which could improve safety of batteries with Li metal anodes to some extent. In general, the GF-LC-modified Li metal anode provides a feasible and promising method to obtain a safe Li metal battery with a longer cycling life.

SUPPLEMENTARY DATA ASSOCIATED WITH THIS ARTICLE

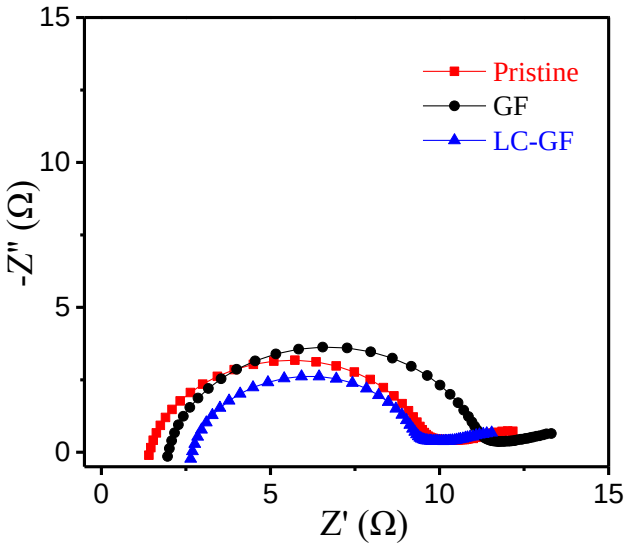

Figure S1. EIS of Li metal symmetric cells with pristine, GF- and LC-GF-modified Li metal electrodes, respectively, before charge/discharge cycling.

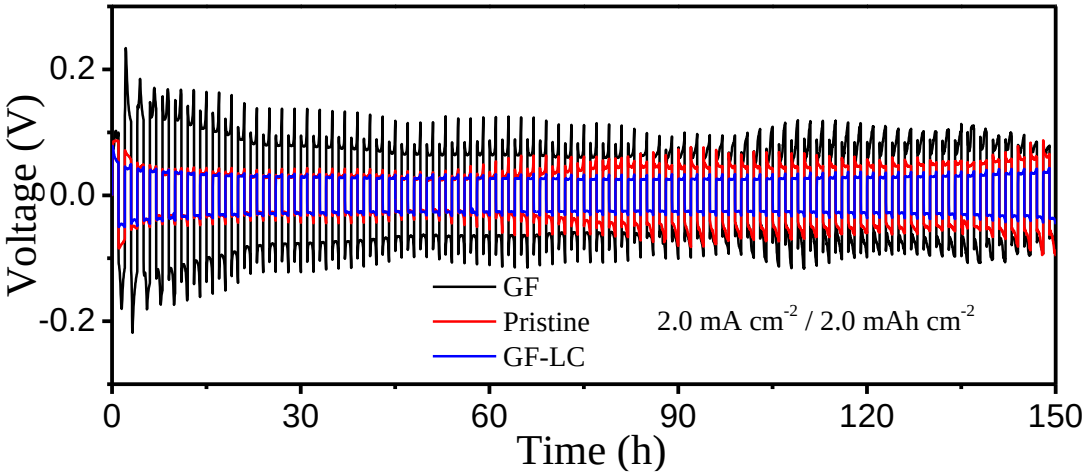

Figure S2. Galvanostatic cycling performance of Li metal symmetric cells with pristine, GF- and GF-LC-modified Li metal anodes at a current density of 2 mA·cm^{-2} for 2 mA·h·cm^{-2}.

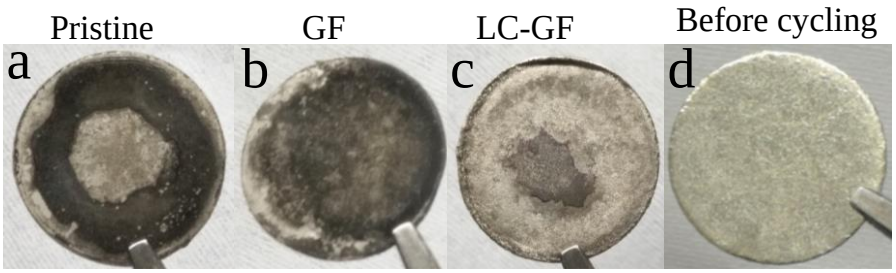

Figure S3. Li metal plates from Li symmetric cells after 180h cycles at different current densities in Fig. 2b modified by pristine (**a**), GF (**b**), LC-GF (**c**) and before cycling (**d**).

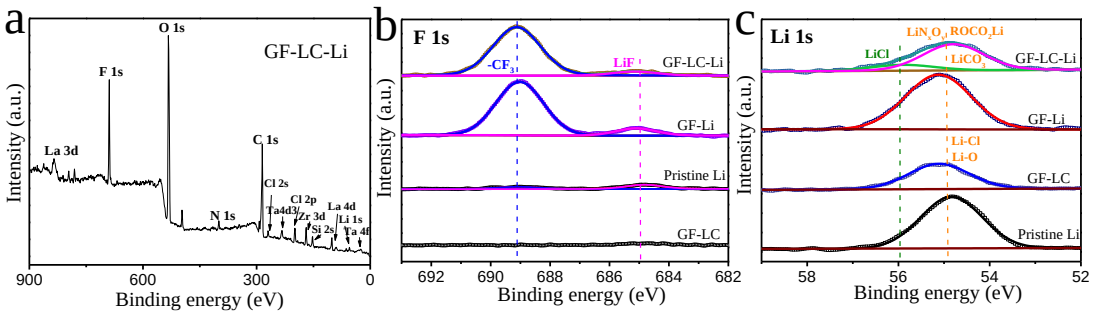

Figure S4. (a) XPS survey spectrum of the GF-LC-modified Li metal surface for symmetric Li metal cell after 1100 h cycling at a current density of 1 mA cm^{-2}. (b) F1s and (c) Li 1s XPS spectra of the pristine, GF-modified, and GF-LC-modified Li metal surfaces for symmetric Li metal cells after 800 h, 1000 h and 1100 h cycling, respectively, at a current density of 1 mA cm^{-2}.

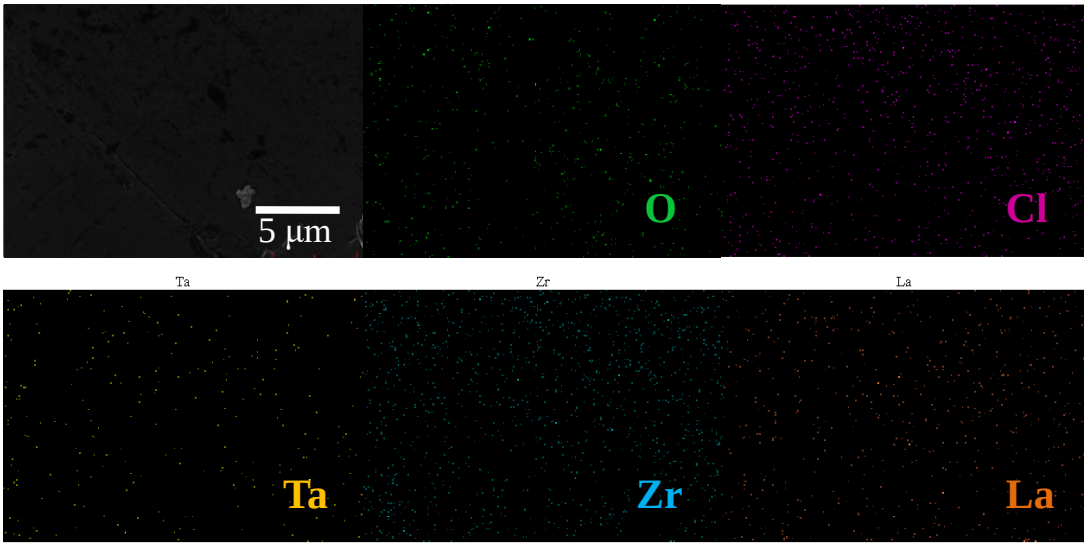

Figure S5. (g) SEM image of Li metal surface for Li symmetric battery after 1100 h cycles and correlating EDX mapping of O, Cl, Ta, Zr and La.

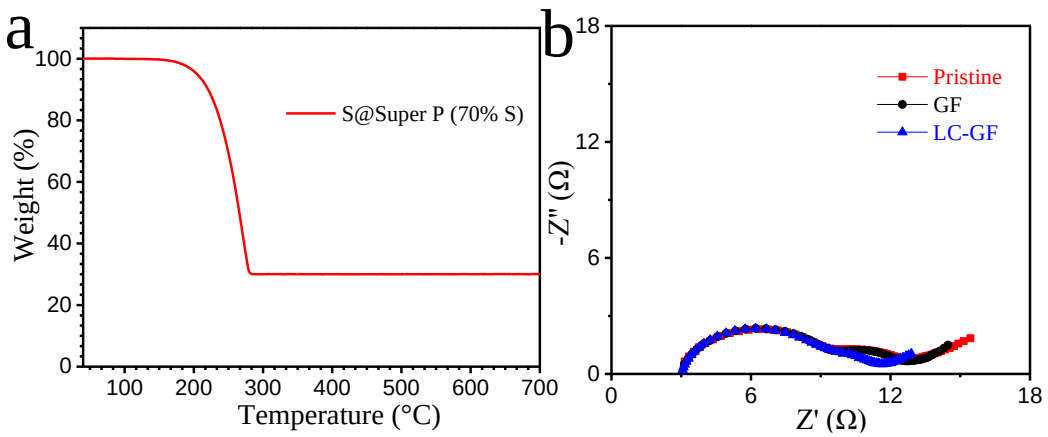

Figure S6. (a) TGA curve of S@Super P composite cathode material. (b) EIS of Li-S cells with pristine, GF- and LC-GF-modified Li metal anodes before charge/discharge cycling, which indicates the existence of GF and GF-LC could not increase resistance of Li-S batteries compared with pristine Li-S battery.

Table 1. Comparison of different strategies for improving performance of room-temperature Li metal electrodes.

Strategies	Li / Li cell			Li / Cu cell			Reference
	Current density (mA cm^{-2} / mAh cm^{-2})	Stable cycle time (h)	Stability of voltage polarization per cycle (side-reactions)	Current density (mA cm^{-2} / mAh cm^{-2})	Cycle time (h)	Coulombic efficiency (%)	

Nitrogen (N) doped grapheme as the Li plating matrix	1.0 / 0.042	12.6	Random voltage oscillations	1.0 / 1.0	~200	98.0	*Angew. Chem. Int. Ed.*. 2017, **56**, 7764-7768.
Glass fiber cloth via even distribution of Li ions	1.0 / 0.1667	~167	Random voltage oscillations	1.0 / 1.0	70	97.0	*Adv. Mater.* 2016, **28**, 2888–2895.
Functional metal–organic framework via chemical interactions	1.0 / 1.0	~800	random voltage oscillations	0.5 / 0.5	~200	99.0	*Chem.Sci.*, 2017, **8**, 4285-4291.
Accommodating lithium into 3D current collectors	0.2 / 0.5	600	random voltage oscillations	0.5 / 1.0	200	98.5	*Nat. Commun.* 2015, **6**, 8058.
GF-LC via in situ reaction interfacial layer	1.0 / 1.0	1100	extremely stable	1.0 / 1.0	300	99.0	This work

ACKNOWLEDGEMENTS

This work was supported by the Foundation of National Key Laboratory of Science and Technology on Power Sources (2016YFB0901700).

References

1. P.G. Bruce, S.A. Freunberger, L.J. Hardwick, and J.-M. Tarascon, *Nat. Mater.*, 11 (2012) 19-29.
2. B. Dunn, H. Kamath, and J.-M. Tarascon, *Science*, 334 (2011) 928.
3. Q. Pang, X. Liang, C.Y. Kwok, and L.F. *Nazar*, Nat.Energy, 1 (2016) 16132.
4. L. Luo, B. Liu, S. Song, W. Xu, J.-G. Zhang, and C. Wang, *Nat. Nanotechnol.*, 12 (2017) 535.
5. W. Xu, J. Wang, F. Ding, X. Chen, E. Nasybulin, Y. Zhang, and J.-G. Zhang, *Energy Environ. Sci.*, 7 (2014) 513-537.
6. K. Zhang, G.-H. Lee, M. Park, W. Li, and Y.-M. Kang, *Adv. Energy Mater.*, 6 (2016) 1600811.
7. A. Manthiram, X. Yu, and S. Wang, *Nat. Rev. Mater.*, 2 (2017) 16103.
8. X.-B. Cheng, R. Zhang, C.-Z. Zhao, F. Wei, J.-G. Zhang, and Q. Zhang, *Adv. Sci.*, 3 (2016) 1500213.
9. K. Yan, H.-W. Lee, T. Gao, G. Zheng, H. Yao, H. Wang, Z. Lu, Y. Zhou, Z. Liang, Z. Liu, S. Chu, and Y. Cui, *Nano Lett.*, 14 (2014) 6016-6022.
10. K.J. Harry, D.T. Hallinan, D.Y. Parkinson, A.A. MacDowell, and N.P. Balsara, *Nat. Mater.*, 13 (2014) 69-73.
11. D. Lu, Y. Shao, T. Lozano, W.D. Bennett, G.L. Graff, B. Polzin, J. Zhang, M.H. Engelhard, N.T. Saenz, W.A. Henderson, P. Bhattacharya, J. Liu, and J. Xiao, *Adv. Energy Mater.*, 5 (2015) 1400993.

12. R. Zhang, X.-R. Chen, X. Chen, X.-B. Cheng, X.-Q. Zhang, C. Yan, and Q. Zhang, *Angew. Chem., Int. Ed.*, 56 (2017) 7764-7768.
13. Y. Liu, D. Lin, P.Y. Yuen, K. Liu, J. Xie, R.H. Dauskardt, and Y. Cui, *Adv. Mater.*, 29 (2017) 1605531.
14. Z. Tu, Y. Kambe, Y. Lu, and L.A. Archer, *Adv. Energy Mater.*, 4 (2014) 1300654.
15. Z. Zhang, Y. Lai, Z. Zhang, K. Zhang, and J. Li, *Electrochim, Acta*, 129 (2014) 55-61.
16. D. Zhou, R. Liu, Y.-B. He, F. Li, M. Liu, B. Li, Q.-H. Yang, Q. Cai, and F. Kang, *Adv. Energy Mater.*, 6 (2016) 1502214.
17. W. Luo, L. Zhou, K. Fu, Z. Yang, J. Wan, M. Manno, Y. Yao, H. Zhu, B. Yang, and L. Hu, *Nano Lett.*, 15 (2015) 6149-6154.
18. W. Liu, Y. Mi, Z. Weng, Y. Zhong, Z. Wu, and H. Wang, *Chem. Sci.*, 8 (2017) 4285-4291.
19. X.-B. Cheng, H.-J. Peng, J.-Q. Huang, R. Zhang, C.-Z. Zhao, and Q. Zhang, *ACS Nano*, 9 (2015) 6373-6382.
20. R. Zhang, X.-B. Cheng, C.-Z. Zhao, H.-J. Peng, J.-L. Shi, J.-Q. Huang, J. Wang, F. Wei, and Q. Zhang, *Adv. Mater.*, 28 (2016) 2155-2162.
21. Y. Zhang, J. Qian, W. Xu, S.M. Russell, X. Chen, E. Nasybulin, P. Bhattacharya, M.H. Engelhard, D. Mei, R. Cao, F. Ding, A.V. Cresce, K. Xu, and J.-G. Zhang, *Nano Lett.*, 14 (2014) 6889-6896.
22. N.-W. Li, Y.-X. Yin, C.-P. Yang, and Y.-G. Guo, Adv. Mater., 28 (2016) 1853-1858.
23. Y. Lu, Z. Tu, and L.A. Archer, *Nat. Mater.*, 13 (2014) 961-969.
24. Y. Lu, M. Tikekar, R. Mohanty, K. Hendrickson, L. Ma, and L.A. Archer, *Adv. Energy Mater.*, 5 (2015) 1402073.
25. M.-T.F. Rodrigues, G. Babu, H. Gullapalli, K. Kalaga, F.N. Sayed, K. Kato, J. Joyner, and P.M. Ajayan, *Nat. Energy*, 2 (2017) 17108.
26. R. Chen, W. Qu, X. Guo, L. Li, and F. Wu, *Mater. Horiz.*, 3 (2016) 487-516.
27. Y. Li, W. Zhou, X. Chen, X. Lü, Z. Cui, S. Xin, L. Xue, Q. Jia, and J.B. Goodenough, Proc. Natl. Acad. Sci. U. S. A., 113 (2016) 13313-13317.
28. Q.-C. Liu, J.-J. Xu, S. Yuan, Z.-W. Chang, D. Xu, Y.-B. Yin, L. Li, H.-X. Zhong, Y.-S. Jiang, J.-M. Yan, and X.-B. Zhang, *Adv. Mater.*, 27 (2015) 5241-5247.
29. T. Zhang, and H. Zhou, *Nat. commun.*, 4 (2013) 1817.
30. H.S. Kato Y, Hori S, Saito T, Suzuki K, Hirayama M, Mitsui A, Yonemura M, Iba H, and Kanno R, *Nat. Energy*, 1 (2016) 16030.
31. X. He, Y. Zhu, and Y. Mo, *Nat. commun.*, 8 (2017) 15893.
32. V.T. R. Murugan, and W. Weppner, *Angew. Chem.*, 119 (2007) 7925 –7928.
33. Han X, Gong Y, Fu K, He X, G. T. Hitz, Dai J, A. Pearse, Liu B, Wang H, G. Rubloff, Y. Mo, V. Thangadurai, E. D. Wachsman, and Hu L, *Nat. Mater.*, 16 (2016) 572-579.
34. W. Luo, Y. Gong, Y. Zhu, K.K. Fu, J. Dai, S.D. Lacey, C. Wang, B. Liu, X. Han, Y. Mo, E.D. Wachsman, and L. Hu, *J. Am. Chem. Soc.*, 138 (2016) 12258-12262.
35. Y. Tian, F. Ding, H. Zhong, C. Liu, Y.-B. He, J. Liu, X. Liu, and Q. Xu, *Energy Storage Materials*, 14 (2018) 49-57.
36. X.-B. Cheng, T.-Z. Hou, R. Zhang, H.-J. Peng, C.-Z. Zhao, J.-Q. Huang, and Q. Zhang, *Adv. Mater.*, 28 (2016) 2888-2895.
37. C. Yang, B. Liu, F. Jiang, Y. Zhang, H. Xie, E. Hitz, and L. Hu, *Nano Research*, 10 (2017) 4256-4265.
38. N.-W. Li, Y.-X. Yin, C.-P. Yang, and Y.-G. Guo, *Adv. Mater.*, 28 (2016) 1853-1858.
39. Y. Zhao and L. L. Daemen, *J. Am. Chem. Soc.*, 134 (2012) 15042-15047
40. Y. Liu, D. Lin, P.Y. Yuen, K. Liu, J. Xie, R.H. Dauskardt, and Y. Cui, *Adv. Mater.*, 29 (2017) 1605531.
41. R. Zhang, X.-R. Chen, X. Chen, X.-B. Cheng, X.-Q. Zhang, C. Yan, and Q. Zhang, Angew. *Chem. Int. Ed.*, 56 (2017) 7764-7768.

42. W. Liu, Y. Mi, Z. Weng, Y. Zhong, Z. Wu, and H. Wang, *Chem. Sci.*, 8 (2017) 4285-4291.